Unravelling DNA organization with single-molecule force spectroscopy using magnetic tweezers

Brouwer, T.B.; Kaczmarczyk, A.P.; Zarguit, I.; Pham, L.; Dame, R.T.; Noort, S.J.T. van

Chapter 25

Unravelling DNA Organization with Single-Molecule Force Spectroscopy Using Magnetic Tweezers

Thomas B. Brouwer, Artur Kaczmarczyk, Ilias Zarguit, Chi Pham, Remus T. Dame, and John van Noort

Abstract

Genomes carry the genetic blueprint of all living organisms. Their organization requires strong condensation as well as carefully regulated accessibility to specific genes for proper functioning of their hosts. The study of the structure and dynamics of the proteins that organize the genome has benefited tremendously from the development of single-molecule force spectroscopy techniques that allow for real-time, nanometer accuracy measurements of the compaction of DNA and manipulation with pico-Newton scale forces. Magnetic tweezers, in particular, have the unique ability to complement such force spectroscopy with the control over the linking number of the DNA molecule, which plays an important role when DNA-organizing proteins form or release wraps, loops, and bends in DNA. Here, we describe all the necessary steps to prepare DNA substrates for magnetic tweezers experiments, assemble flow cells, tether DNA to a magnetic bead inside a flow cell, and manipulate and record the extension of such DNA tethers. Furthermore, we explain how mechanical parameters of nucleoprotein filaments can be extracted from the data.

Key words Magnetic tweezers, Single molecule, Force spectroscopy, Rotational spectroscopy, DNA mechanics, DNA compaction, Bacterial chromatin, Archaeal chromatin, Eukaryotic chromatin

1 Introduction

1.1 Chromatin Organization by DNA-Binding Proteins

Genomes carry the genetic blueprint of all living organisms. Their organization requires strong condensation in a structure called chromatin, as well as carefully regulated accessibility to genes in chromatin for the proper functioning of their hosts. The organization of chromatin is carried out by a large group of proteins that vary in abundance, structure, and function. Different kingdoms of life have evolved to implement different solutions for a compact but dynamic organization of chromatin. Nonetheless, many of the involved proteins share common mechanisms to deform the DNA by inducing kinks, bends, wraps, and loops in the DNA trajectory.

Remus T. Dame (ed.), *Bacterial Chromatin: Methods and Protocols*, Methods in Molecular Biology, vol. 2819,
https://doi.org/10.1007/978-1-0716-3930-6_25,

Examples of common DNA-organizing proteins are histone proteins found in eukaryotes, in archaea, and recently also in some bacterial species [1–5]. Proteins like histone-like protein from strain U93 (HU), integration host factor (IHF), and histone-like nucleoid-structuring protein (H-NS) are more commonly found in bacteria [6].

For a mechanistic understanding of the function of these proteins, required for a robust comprehension of chromatin-associated processes such as transcription, a detailed knowledge of the kinetics of DNA binding, as well as the mechanical consequences of their binding to DNA, is required. In fact, there is a tight relationship between DNA conformation and its interaction with proteins: wrapping of DNA around proteins results in condensation of the DNA, both by bringing together the ends of the DNA and by inducing supercoiling in the surrounding DNA, which results in additional condensation by plectoneme formation. DNA supercoiling, induced by externally applied torque, will facilitate the binding of proteins that wrap or bend the DNA with similar chirality. Force and extension play similar related roles: some proteins induce stretching of DNA upon binding. Pre-stretching of DNA can facilitate the binding or function of these proteins, making force an important parameter in the study of nucleoprotein filaments [7].

DNA forms the common thread in chromatin organization, and it is informative to gather and compare mechanochemical experimental data on chromatin organization by different proteins and from various species, to gather a comprehensive picture of DNA organization. In terms of DNA mechanobiology, as well as from an evolutionary perspective, it is highly desirable to establish a physical understanding of chromatin organization throughout the kingdoms of life. In this chapter, we present protocols to set up single-molecule force spectroscopy experiments on DNA tethers interacting with a variety of chromatin proteins originating from bacteria, archaea, and eukaryotes. It is our experience that the methods for sample preparation, execution of the experiments, and data analysis are similar, and we provide protocols that can be used to study bacterial and archaeal chromatin, as well as other nucleoprotein complexes.

1.2 Magnetic Tweezers

The introduction of single-molecule biophysical assays has boosted our understanding of the mechanical properties of DNA-binding proteins. Where conventional ensemble experiments are limited by averaging multiple populations and dynamic conformations, single-molecule biophysical assays do not suffer from this restriction. For instance, Tethered Particle Motion (TPM) experiments revealed that binding of the bacterial genome-organizing protein IHF yields two subpopulations at low concentrations of IHF (*see* Chapter 23), representing a bound and unbound state. Even though TPM

experiments provide great insight into the molecular mechanisms of biomolecules, the application of either or both force and twist/torque can provide extra information to uncover protein-induced conformational changes of DNA. Magnetic tweezers (MT), in particular, can probe the mechanical response of individual biomolecules to applied force and twist. The first MT experiments have been instrumental in understanding the mechanical behavior of bare DNA [8–10]. Since then, mechanical and structural properties of more complex biomolecules and DNA–protein complexes have been studied [10–16]. MT are especially suitable to this end since they require limited hardware investments, uniquely control both force and linking number, and have a relatively high throughput compared to optical tweezers, the most common alternative single-molecule force spectroscopy technique. Recent developments are an increase in maximum force to beyond the overstretching force for DNA [13, 17, 18], multiplexing capabilities, such that hundreds of molecules can be measured in parallel [19–21], and freely orbiting magnetic tweezers (FOMT) [22] or magnetic torque tweezers (MTT) [23] that allow for (partial) relief of twist or direct torque measurement. Another advance is the replacement of permanent magnets by electromagnets in electromagnetic tweezers [10, 24]. Since there are no moving parts in electromagnetic tweezers, the only factor limiting the speed of the experiments is the viscous drag of the magnetic beads themselves. Finally, combinations with (single-molecule) fluorescence have been reported [25–28]. These modern variations of the technique require similar sample preparation protocols and can be seen as extensions of typical MT experiments.

A typical MT experiment involves a single DNA molecule tethered between a paramagnetic bead and a functionalized glass slide. The three-dimensional position of the bead is recorded in time by video microscopy and extracted by image processing. The bead can be manipulated by translation or rotation of a pair of magnets that are held above the tether. The force and torque that are exerted on the paramagnetic bead result in a restoring force and torque in the tethered molecule, which provides insight into the structure of the tether.

1.3 Measurement Schemes

MT can be operated in several measurement schemes. Traditionally, the magnet is fixed in a preset position during a measurement, resulting in a constant force during the experiment. For bare DNA, such a constant force measurement not only accurately reveals the extension of the tether, but one can also directly calculate the force by quantification of the lateral movements of the bead [9]. Application of the equipartition theorem yields that the force must equal the product of thermal energy and extension, divided by the variance of the lateral fluctuations (*see* Subheading 3.7).

Repeated measurements at different magnet positions yield a calibration of the force as a function of the magnet position [9, 29–32], which typically follows a mono- or bi-exponential decay [31]. The same measurement also provides an accurate map of the force–extension relation of DNA, which can be described by a wormlike chain (WLC) model. For transient protein–DNA interactions, a constant force experiment can directly reveal changes in extension of the tether upon flushing the protein solution in or out [33–35].

Having established a force calibration relation, one can revert to dynamic force spectroscopy, in which the extension of the tether is monitored during repositioning of the magnet [36]. Such a measurement scheme aids in revealing the force dependence of structures that may rupture or dissociate when increasing forces are applied. For instance, we have noticed that eukaryotic histone proteins readily dissociate when chromatin fibers are exposed to forces exceeding several pN [16].

Next to shifting the position of the magnets with respect to the tethered bead, the magnets can be rotated around the axis of the tether. Since the torque on the bead is proportional to the strength of the magnetic field (*see* **Note 1**) and is typically much larger than the opposing torque provided by the DNA tether, the bead will immediately follow the rotation of the magnets. This can lead to accumulation of twist in the tether, if the twist is not relieved by swiveling around the bond between the tether and bead or surface or by swiveling around a nick in the DNA. Constraining the rotation of the DNA ends requires more than one chemical bond between the DNA strand and the bead or surface, which can be achieved by introducing multiple affinity tags in the DNA ends. Such a DNA substrate allows for direct control of the linking number of the topological domain formed by the bead and the surface. Here, we describe the preparation of both torsionally constrained and torsionally free DNA substrates, allowing for a broad spectrum of applications.

Controlling the linking number of the DNA tether opens up a range of measurement schemes. At constant twist, force–extension measurements can be done in a similar fashion as with torsionally unconstrained DNA. Any twist–stretch coupling will be evident in the force–extension curve. Protein-induced (un)wrapping will accumulate, which may affect the binding of subsequent proteins. A torsionally constrained tether can be pre-twisted before force spectroscopy experiments, to probe the chiral properties of the tether over a wide range of linking numbers [37]. The mechanical response of the tether to torque can also be measured directly by twisting the tether under constant force. In conclusion, a wide variety of single-molecule manipulation schemes is available with MT force spectroscopy.

1.4 Data Analysis

The mechanical properties of DNA provide a reference for data analysis of nucleoprotein filaments. The extension of DNA as a function of force can be described accurately by the WLC model [38]. At forces larger than 10 pN, the extensible WLC model provides a better fit [38, 39]. DNA extension as a function of twist requires a more elaborate analysis, using numerical methods, due to the coexistence of three conformations, i.e., twisted, melted, and plectonemic DNA [37]. However, for force and twist regimes where only two of these states prevail, analytical solutions exist [40]. In general, it is important to make sure that the force–extension curves of bare DNA, under conditions relevant for studying chromatin, fit well to these models, prior to the study of more advanced structures, as protein-induced changes in extension can be difficult to interpret without proper reference.

Wrapping, bending, twisting, or deforming DNA otherwise will result in a change in extension of the tether that may depend on force and twist. In a force–extension curve, this may lead to a change in persistence length, contour length, stretch modulus, and/or twist persistence length. In the data analysis part of the methods section, we review some models that can be fitted to extract these parameters, as well as more dynamic methods to extract the kinetics of protein binding.

Below, we describe in detail how to make DNA substrates suitable for MT. Note that many variations of DNA substrates exist that the reader can adapt to specific needs. We report a detailed protocol for the assembly of DNA-tethered beads in a flow cell, ready for measurements, and share some typical procedures for data analysis. These should provide a solid foundation to study chromatin at the single-molecule level with MT.

2 Materials

2.1 Stock Solutions

All aqueous buffers are prepared with ultrapure Milli-Q water and stored at 4 °C.

1. Measurement buffer: 10 mM HEPES pH 7.5, 100 mM KCl, 10 mM NaN_3 (sodium azide), 0.2% bovine serum albumin (BSA) (heat shock fraction, pH 7, ≥98%), and 0.1% TWEEN 20 (*see* **Note 2**).
2. Passivation buffer: 10 mM sodium azide, 3.6% BSA, and 0.1% TWEEN 20 (*see* **Note 2**).

2.2 Isolation of DNA Plasmids

1. Desired DNA plasmid (*see* **Note 3**).
2. XL1-Blue Competent Cells.
3. Heat block, such as the Eppendorf ThermoMixer.

4. Orbital shaker.
5. Microcentrifuge, such as the Eppendorf 5424R.
6. Lysogeny broth (LB) medium (*see* **Note 4**).
7. LB agar plates (*see* **Note 4**).
8. 500-mL Erlenmeyer flask.
9. DNA plasmid isolation kit, such as the NucleoBond Xtra Midi kit.

2.3 Digestion and Labeling of DNA

1. Isolated DNA plasmid (*see* **Note 3**).
2. Restriction enzymes (*see* **Note 3**).
3. Reaction buffer for digestion.
4. DNA purification kit, such as the Wizard SV Gel and PCR cleanup kit.
5. Spectrophotometer for micro-volume concentration measurement of nucleic acids, for instance, the BioDrop μLITE.
6. Agarose for DNA/RNA electrophoresis.
7. Horizontal electrophoresis system.
8. dNTPs (100 mM).
9. DNA ladder.
10. Ethidium bromide (10 mg/mL).
11. Klenow fragment.
12. Reaction buffer for Klenow fragment.
13. Digoxigenin-labeled ddUTP (1 mM).
14. Biotin-labeled ddUTP (1 mM).
15. DNA plasmid as a template for DNA handles (*see* **Note 3**).
16. Forward primer to construct DNA handles (*see* **Note 3**).
17. Backward primer to construct DNA handles (*see* **Note 3**).
18. T4 DNA ligase.
19. Reaction buffer for T4 DNA ligase.
20. DNA PCR kit, such as the FastStart Taq DNA polymerase kit.
21. Digoxigenin-labeled dUTP (1 mM).
22. Biotin-labeled dUTP (1 mM).
23. Sodium dodecyl sulfate (SDS) ≥98.5% (GC).
24. PCR thermal cycler, such as the Bio-Rad T100.
25. UV transilluminator, such as the Bio-Rad UVT 2000.
26. Imaging system for visualization of electrophoresis gels, such as the ChemiDoc Imaging Systems.

2.4 Flow Cell Assembly

1. High-precision crossover tweezers.
2. Carbon steel scalpel.
3. N_2 spray gun.
4. 2-Propanol.
5. Custom-built flow cell body.
6. Frame.
7. Coverslip 24 × 40 mm (#1.5 thickness).
8. Coverslip 24 × 60 mm (#1.5 thickness).
9. Parafilm.
10. Ultrasonic cleaning bath.
11. Glass staining trough.
12. 100-mL glass beaker.

2.5 Bead–Tether Assembly

1. DNA substrate (torsionally constrained or torsionally free).
2. Magnetic rack for bead separation.
3. Streptavidin-coated paramagnetic beads (*see* **Note 5**).
4. Nitrocellulose 1% in amyl acetate.
5. Pentyl acetate (amyl acetate) puriss. p.a., ≥98.5% (GC).
6. Anti-digoxigenin (AD).

2.6 Microscope

1. Microscope objective (flat field, NA = 1.3, 40×, oil immersion, field number 25).
2. CMOS camera (25 Mpix, 8 bit, 30 fps, Camera Link Full interface).
3. Infinity-corrected tube lens ($f = 200$ mm).
4. Kinematic pitch/yaw adapter.
5. LED collimator ($\lambda = 645$ nm, 100 μW, 20 mA).
6. Frame grabber for Camera Link Full interface.
7. Multi-core PC (e.g., 10-core) with 32-GB DDR3 memory.
8. XYZ piezo stage (20 μm travel in Z [0.1-nm resolution]).
9. Cube magnets (N50 magnetized, 5 mm).
10. Stepper motor controller (6-axis, 1–256 micro-steps).
11. Hollow-shaft stepper motor (2-phase, NEMA 8).
12. Two translation stages to mount objective and magnets (20-mm travel [0.1 μm resolution]).
13. XY manual positioning stage (20-mm travel in XY, 65-mm aperture).
14. Ø1″ and Ø2″ broadband dielectric mirrors ($\lambda = 400$–750 nm).

3 Methods

3.1 Isolation of DNA Plasmids

1. Take 100 μL of XL1-Blue Competent Cells (at a concentration of approximately 3×10^8 cells/mL) from the −80 °C freezer and let thaw on ice (*see* **Note 6**). Add approximately 1.0 μL of the desired DNA plasmid (*see* **Note 7**) to the Eppendorf tube, gently mix, and incubate on ice for a minimum of 30 min.
2. Heat-shock the sample for 90–120 s at 42 °C by means of the thermomixer. Do not shake the sample or exceed the indicated time.
3. Place the tube back on ice for 60 s and add 900 μL of LB medium. Gently shake (240 rpm) and incubate the tube for 30–60 min at 37 °C.
4. Centrifuge the tube for 60 s at 20,000*g*, remove approximately 90% of the supernatant, and resuspend the sample.
5. Spread the sample on a LB agar plate containing the appropriate antibiotic (here: ampicillin) and incubate (upside down) at 37 °C overnight.
6. Pick up one colony and put it into a 500-mL Erlenmeyer flask containing 250-mL LB medium and the appropriate antibiotic (here: ampicillin). Incubate on the shaker (320 rpm) at 37 °C overnight.
7. Isolate and purify the plasmid DNA with NucleoBond® Xtra Midi kit (Macherey-Nagel) following the manufacturer's protocol.

3.2 Production of Torsionally Free DNA

1. Digest the DNA plasmid by mixing the reagents listed in Table 1 in an Eppendorf tube and incubate at 37 °C overnight (*see* **Notes 8** and **9**).
2. Inactivate BsaI by incubating for 20 min at 65 °C (*see* **Note 10**).
3. Purify DNA with Promega Wizard SV Gel and PCR cleanup kit following the manufacturers' protocol (*see* **Notes 11** and **12**). Determine the DNA concentration after purification by measuring A_{260} (absorbance at 260 nm) with the spectrophotometer and store a microliter of the reaction mixture for agarose gel electrophoresis.
4. Label one end of the digested DNA by mixing the reagents listed in Table 2 in an Eppendorf tube and incubate at 37 °C for 2 h (*see* **Note 13**). The end concentration of (labeled) dNTPs should be 20 μM (*see* **Note 14**). Note that in this step the DNA is labeled with ddUTP rather than dUTP (*see* **Note 15**).
5. Purify DNA and store a microliter of reaction mixture for agarose gel electrophoresis.

Table 1
Composition of digestion reaction mixture I, used for preparation of the torsionally free construct

pUC18 DNA plasmid (with 601-array) (2000 ng/μL)	20 μL	40 μg
NEBuffer 3.1 (10× concentrated)	80 μL	–
Milli-Q water	696 μL	–
BsaI (10 U/μL)	4 μL	40 units
Total volume	*800 μL*	

Table 2
Composition of labeling reaction mixture I, used for preparation of the torsionally free construct

BsaI-digested pUC18 DNA (with 601-array) (400 ng/μL)	50 μL	20 μg
Reaction buffer for Klenow fragment (10× concentrated)	10 μL	–
Digoxigenin – 11 – ddUTP (1 mM)	2 μL	20 μM
dGTP (1 mM)	2 μL	20 μM
dCTP (1 mM)	2 μL	20 μM
Milli-Q water	24 μL	–
Klenow fragment, LC (2 U/μL)	10 μL	20 units
Total volume	*100 μL*	

Table 3
Composition of DNA plasmid digestion reaction mixture II, used for preparation of the torsionally free construct

Single-labeled pUC18 DNA (with 601-array) (200 ng/μL)	50 μL	10 μg
NEBuffer 3.1 (10× concentrated)	20 μL	–
Milli-Q water	128 μL	–
BseYI (5 U/μL)	2 μL	10 units
Total volume	*200 μL*	

6. Digest the DNA labeled in the previous steps with a single digoxigenin by mixing the reagents listed in Table 3 in an Eppendorf tube and incubate at 37 °C overnight.
7. Inactivate BseYI by incubating for 20 min at 80 °C.
8. Purify DNA and store a microliter of reaction mixture for agarose gel electrophoresis.
9. Label the second extremity of the DNA by mixing the reagents listed in Table 4 in an Eppendorf tube and incubate at 37 °C for 2 h.

Table 4
Composition of labeling reaction mixture II, used for preparation of the torsionally free construct

BseYI-digested single-labeled pUC18 DNA (with 601-array) (150 ng/μL)	50 μL	7.5 μg
Reaction buffer for Klenow fragment (10× concentrated)	10 μL	–
Biotin – 16 – ddUTP (1 mM)	2 μL	20 μM
dCTP (1 mM)	2 μL	20 μM
Milli-Q water	32.25 μL	–
Klenow fragment, LC (2 U/μL)	3.75 μL	7.5 units
Total volume	*100 μL*	

10. Purify DNA and store a microliter of reaction mixture for agarose gel electrophoresis.
11. Check the digestion reaction products by electrophoresis using a 1% agarose gel. Pre-stain the gel with ethidium bromide by diluting the stock 10,000× in the agarose solution before it cures (*see* **Note 16**). Load the gel with the products obtained at different steps of the labeling procedure, flanked by two DNA ladders. Load approximately 50–100 ng of DNA per lane. Run the gel in TBE buffer in a horizontal electrophoresis system for 1–2 h at 90 mV or until bands are adequately separated. Visualize the electrophoresis gel in an imaging system adjusted for ethidium bromide staining.

Alternatively, it is possible to use PCR with biotin- and digoxigenin-labeled primers, to produce the fragment of interest. After isolating the plasmid (*see* Subheading 3.1), perform a PCR reaction according to the steps below.

1. Make a PCR reaction mixture with the Phusion master mix (Thermo Fisher Scientific) according to the scheme below:

Milli-Q	10.2 μL
5× HF buffer (Thermo Fisher Scientific)	4 μL
2 mM dNTPs	2 μL
12.5 μM forward primer	1 μL
12.5 μM reverse primer	1 μL
Template (plasmid)	1 μL
DMSO (3% v/v)	0.6 μL
Phusion PCR mix (Thermo Fisher Scientific)	0.2 μL
Total	20 μL

2. Perform a standard PCR using the manufacturer's protocol. Alternatively if the primers have a high annealing temperature or if the difference between the annealing and extension temperature is small, it is possible to perform a 2-step PCR, which combines the annealing and extension into one step, as described below.

Temperature in Celsius	Time in minutes	Phase
98	1:00	Initial denature
98	0:30	Denature
72	30 s/kb DNA	Annealing /extension
72	10:00	Final extension
12	Hold	Hold

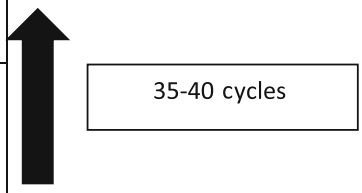

3. To get an idea of the yield as well as the presence of any unwanted side product, we load 1 μL of product on a 1% agarose gel. Pre-stain the gel with ethidium bromide or GelRed by diluting the stock 10.000× in the agarose solution before it cures (*see* **Note 16**). Run the gel for 1–2 h on 90 V depending on the expected DNA size. Image the gel using a Gel Doc XR+ (Bio-Rad) (*see* **Note 17**).
4. To remove template DNA from the PCR product, add 1 μL of DpnI (ten units) to the reaction mixture and incubate at 37 °C for 1 h (*see* **Note 18**).
5. Separate the PCR products by electrophoresis using a 1% agarose gel. Pre-stain the gel with ethidium bromide or GelRed by diluting the stock 10,000× or 1000×, respectively, in the agarose solution before it cures (*see* **Note 16**). Load the PCR products in a large slot, obtained by using 1.0-mm comb and merging several lanes together (with tape), flanked by two DNA ladders.
6. Image the gel on the UV transilluminator to locate the bands of interest. Minimize the time on the UV transilluminator (*see* **Note 19**). To separate the construct of interest from the DNA template and undesired side products, use a scalpel to excise the desired DNA band from the gel.
7. Purify the digested DNA from gel with the Promega Wizard SV Gel and PCR cleanup kit following the manufacturer's protocol (*see* **Note 20**).

Table 5
Composition of the reaction mixture for digestion of the DNA plasmid for the torsionally constrained construct

pUC18 DNA plasmid (with 601-array) (2000 ng/μL)	50 μL	100 μg
NEBuffer 3.1 (10× concentrated)	200 μL	–
Milli-Q water	1720 μL	–
BsaI (10 U/μL)	10 μL	100 units
BseYI (5 U/μL)	20 μL	100 units
Total volume	*2000 μL*	

3.3 Production of Torsionally Constrained DNA

1. Digest the DNA plasmid by mixing the reagents listed in Table 5 in an Eppendorf tube and incubate at 37 °C overnight (*see* **Notes 8** and **9**).
2. Inactivate restriction enzymes by incubating for 20 min at 80 °C.
3. Separate the digestion products by electrophoresis using a 1% agarose gel. Pre-stain the gel with ethidium bromide by diluting the stock 10.000× in the agarose solution before it cures (*see* **Note 16**). Load the digested DNA in a large slot, obtained by using a 1.0-mm comb and merging several lanes together (with tape), flanked by two DNA ladders. Before loading, add SDS to an end concentration of 0.5% (*see* **Note 21**).
4. Image the gel on the UV transilluminator to locate the bands of interest. Minimize the time on the UV transilluminator (*see* **Note 19**). To separate the construct of interest from the DNA template and undesired side products, use a scalpel to excise the desired DNA band from the gel.
5. Purify the digested DNA from gel with the Promega Wizard SV Gel and PCR cleanup kit following the manufacturer's protocol (*see* **Note 20**).
6. Construct two sets of handles with multiple biotin or digoxigenin affinity tags by polymerase chain reaction (PCR) (*see* **Notes 22** and **23**). Mix the reagents listed in Table 6 in two separate Eppendorf tubes and place them in the thermal cycler. Use the PCR program depicted in Table 7 and store the tubes at 4 °C. Here, the DNA is labeled with dUTP rather than ddUTP (*see* **Notes 15** and **24**).
7. Digest the biotin PCR product with BsaI and the digoxigenin PCR product with BseYI by mixing the reagents listed in Table 8 in two different Eppendorf tubes and incubate at 37 °C overnight.

Table 6
Composition of the PCR mixture for production of DNA handles for the torsionally constrained construct

Template pUC18 DNA plasmid (100 ng/μL)	1 μL	100 ng
FastStart Taq DNA polymerase (5 U/μL)	0.5 μL	2.5 units
Forward primer to construct DNA handles (10 μM)	1 μL	100 nM
Backward primer to construct DNA handles (10 μM)	1 μL	100 nM
PCR reaction buffer + $MgCl_2$ (10× concentrated)	10 μL	
dNTP (10 mM)	1 μL	100 μM
Biotin – 16 – dUTP (1 mM) or Digoxigenin – 11 – dUTP (1 mM)	1 μL	10 μM
Milli-Q water	84.5 μL	
Total volume	*100 μL*	

Table 7
PCR program to produce the DNA handles

Step	Temperature (°C)	Time (s)	Function
1	95	240	Melt the DNA
2	95	30	Melt the DNA
3	50	45	Anneal the primer to the ssDNA
4	72	60	Elongation by DNA polymerase
5	72	300	Fill in any protruding ends

Steps 2–4 are cycled 30 times

Table 8
Composition of the digestion reaction mixture for generation of the DNA handles of the torsionally constrained construct

Multi-biotin PCR product or multi-digoxigenin PCR product (200 ng/μL)	100 μL	20 μg
NEBuffer 3.1 (10× concentrated)	100 μL	–
Milli-Q water	798 μL or 796 μL	–
BsaI (10 U/μL) or BseYI (5 U/μL)	2 μL or 4 μL	20 units
Total volume	*1000 μL*	

Table 9
Composition of the ligation reaction mixture to produce the torsionally constrained construct

Digested pUC18 DNA (with 601-array) (100 ng/μL)	300 μL	30 μg
Digested multi-biotin PCR product (100 ng/μL)	50 μL	5 μg
Digested multi-digoxigenin PCR product (100 ng/μL)	50 μL	5 μg
T4 DNA ligase reaction buffer (10× concentrated)	80 μL	–
Milli-Q water	315 μL	–
T4 DNA ligase (400 U/μL)	5 μL	2000 units
Total volume	*800 μL*	

8. Inactivate restriction enzymes by incubating for 20 min at 80 °C.
9. Purify digested PCR products with the Promega Wizard SV Gel and PCR cleanup kit following the manufacturers' protocol (*see* **Notes 12** and **25**).
10. Ligate the digested DNA plasmid with the digested PCR products containing the multiple biotin or digoxigenin affinity tags. The digested DNA and PCR products are mixed in equimolar ratio. Mix the reagents listed in Table 9 in an Eppendorf tube and incubate at 4 °C overnight. Before ligase is added, store a microliter of reaction mixture for agarose gel electrophoresis (*see* **Notes 26** and **27**).
11. Inactivate T4 ligase by incubating for 20 min at 65 °C.
12. Purify ligated DNA with the Promega Wizard SV Gel and PCR cleanup kit following the manufacturer's protocol (*see* **Notes 12** and **25**) and elute at least two times (*see* **Note 28**). Store a microliter of reaction mixture for agarose gel electrophoresis.
13. Check the ligation reaction by electrophoresis using a 1% agarose gel. Pre-stain the gel with ethidium bromide by diluting the stock 10.000× in the agarose solution before it cures (*see* **Note 16**). Load the gel with unligated and ligated reaction products, flanked by two DNA ladders. Load approximately 50–100 ng of DNA per lane. Run the gel in TBE buffer in a horizontal electrophoresis system for 1–2 h at 90 mV or until bands are adequately separated. Visualize the electrophoresis gel in an imaging system adjusted for ethidium bromide staining.

3.4 Flow Cell Assembly

1. Put 24 × 60 mm coverslips in a glass staining trough and sonicate in ultrasonic cleaning bath for 15 min in 2-propanol. Dry the coverslips in a stream of N_2 or allow the coverslips to dry in air.

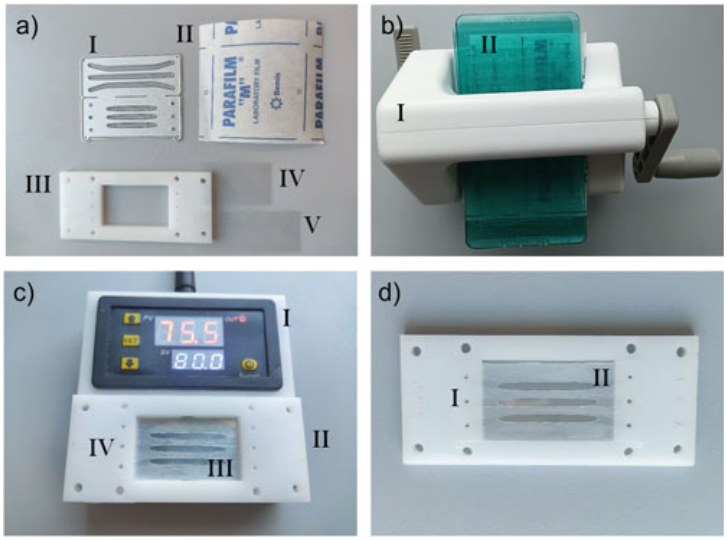

Fig. 1 Assembly of a flow cell. (**a**) The flow cell consists of a laser-cut polyacetal flow cell frame (III), two layers of parafilm (II) that are cut using a custom-made cutting die (I), and a 24 × 40-mm (IV) and a 24 × 60-mm (V) cover slide. The latter is treated with nitrocellulose. (**b**) A sandwich of a green plastic plate, the cutting die, a piece of parafilm (protective paper facing up from the cutting die), and a second green plastic plate (II) is pressed through a Sizzix Sidekick die cutting machine (I). (**c**) The cut parafilm is separated from the protecting paper, folded and carefully pressed onto the flow cell frame (IV, make sure that the entry/exit holes are aligned), and mounted on top of the 24 × 60-mm cover slide (nitrocellulose coated side up), which is placed on a 0.15-mm deep recess of a custom-made heating block. The 24 × 40-mm cover slide is placed into the rectangular cavity of the flow cell frame (III) and gently pressed onto the melting parafilm. When the heating control unit (I) is set to 80 °C, the parafilm melts within 30 s, sealing the channels of the flow cell. (**d**) Bottom view of the flow cell, showing three separate channels (II) and six entry/exit holes (I). Additional larger holes are for alignment and mounting onto the microscope

2. Put 5 mL of 0.1% nitrocellulose in amyl acetate in a 100-mL glass beaker. Using reverse action tweezers, place two of the sonicated coverslips into the beaker directly next to each other. Capillary forces will fill the gap between the two slides with nitrocellulose solution and will quickly coat the coverslip (*see* **Note 29**).
3. Once the gap between the coverslips is filled, use reverse action tweezers to carefully separate the coverslips. Dry the coverslip in a stream of N_2. The coated coverslip can be stored for later use.
4. To assemble a functional flow cell, the following parts are needed: a laser-cut polyoxymethylene flow cell frame (*see* Fig. 1a-III), a nitrocellulose treated glass as prepared in the previous step (Fig. 1a-V), a home-made heating element, and a Sizzix Sidekick die cutting machine (https://www.sizzix.com/661770/sizzix-sidekick-starter-kit-white-gray) (Fig. 1b-I) with a custom-made metal cutting die (*see* Fig. 1a-I).

5. Cut a piece of parafilm and put it, protective paper side up, on top of the metal cutting die. Sandwich the frame and the parafilm between the two plastic plates and pass it through the cutting machine (*see* Fig. 1b). To ensure that the frame cuts the parafilm correctly, it is recommended to pass the sandwich through the cutting machine multiple times. Alternatively, the parafilm can be laser cut or cut manually with a scalpel knife and an appropriate mask.
6. Fold the parafilm in the middle, creating three flow channels, and place the parafilm on top of the polyoxymethylene flow cell frame. Align the holes of the parafilm with the holes of the flow cell frame. Subsequently, place the nitrocellulose-treated 24 × 60 mm glass slide on top of the heating element, which is set at 80 °C (*see* Fig. 1c). Place the plastic frame including the parafilm on top of the glass slide and place a glass coverslip of 24 × 40 mm in the rectangular cavity of the flow cell frame. Evenly apply slight pressure on the smaller coverslip with a rectangular piece of plastic until the parafilm melts and turns from opaque to transparent. Remove the flow cell from the heating element and let it cool for at least 30 s. After cooling, the flow cell is ready for use (*see* Fig. 1d).

3.5 Bead–Tether Assembly

1. Carefully flush the flow cell with 1 mL of Milli-Q water using a pipette and incubate for approximately 30 s. Alternatively, a peristaltic pump can be used to flush the flow cell at 500 μL/min (*see* **Note 30**).
2. Replace the Milli-Q water with 300 μL of 10 ng/μL anti-digoxigenin solution. Incubate at 4 °C for 2 h.
3. Passivate the flow cell by flowing in 1 mL of passivation buffer. Incubate at 4 °C overnight (*see* **Note 31**).
4. Flush the flow cell with 1 mL of measurement buffer.
5. Dilute 1 ng of DNA in 500 μL measurement buffer. Flush the flow cell with DNA and incubate at room temperature for 10 min (*see* **Note 32**).
6. Vortex and wash 1 μL of 1 μg/μL paramagnetic beads in Milli-Q water by means of the magnetic rack according the manufacturer's protocol and dilute the paramagnetic beads in 500 μL measurement buffer. Flush the flow cell with beads and incubate at room temperature for 10 min (*see* **Note 33**).
7. Slowly flush out the excess beads from the flow cell with 500 μL of measurement buffer. The flow cell is now ready for measurements on bare DNA or incubation with DNA binding proteins.

As an alternative to the protocol described above, it is possible to use the TPM protocol as described in Chapter 22.

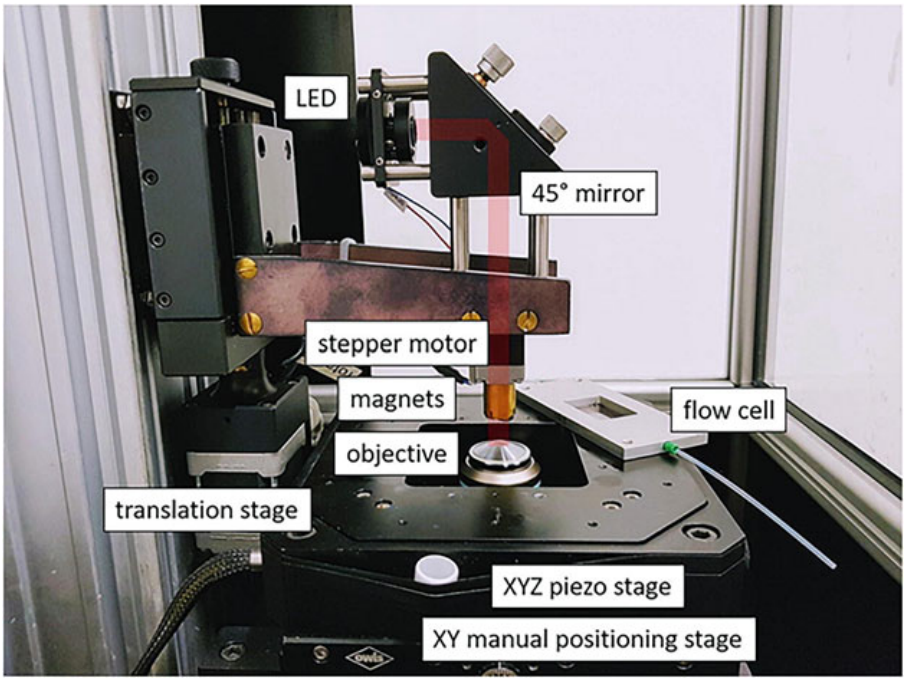

Fig. 2 The magnetic tweezers setup. A collimated LED is mounted in the kinematic pitch/yaw adapter and coupled into a hollow-shaft stepper motor by a Ø1″ mirror. The incoming light passes between a pair of magnets into the objective. The flow cell is mounted on top of an XYZ piezo stage, above the objective (here, the flow cell is shifted to the side for clarity). The piezo stage is mounted on top of an XY manual positioning stage, for coarse movements. The magnets and objective are mounted onto two translation stages. Below the objective, the light is coupled into the camera through an infinity-corrected tube lens by means of a Ø2″ mirror. The light path is depicted in red

3.6 Initial Bead Selection and Height Calibration

1. Position the magnets at such a distance that force is negligible. In our setup, depicted in Fig. 2 (*see* **Note 34**), we position the magnets at least 10 mm above the sample, resulting in a force lower than 0.05 pN.
2. Place the flow cell containing the (preincubated) sample onto the microscope.
3. Put the beads in focus using the objective mounted onto the stepper motor. With the piezo stage, move the objective 10 μm above focus so distinct diffraction rings appear around the beads (*see* **Note 35**).
4. Select regions of interest (ROIs) of 150 × 150 pixels containing single, isolated beads (*see* **Note 36**).
5. Identify an immobile bead as reference bead and use this bead for phase calibration. Move the bead 20 μm in Z while cross-correlating the bead images with a set of computer-generated reference images [21]. Calibrate the phase of the cross-correlation peak with bead height. When there are no immobile beads in the field of view, phase calibration can also be done at an intermediate force, i.e., 1 pN, to reduce the thermal fluctuations of the tethered bead while keeping the tether intact.

6. Once the measurement plane is set and phase calibration is complete, assign the ROIs to tethered beads (manually or by a bead-finding algorithm).
7. Start tracking the beads (*see* **Notes 37** and **38**).

3.7 Force Calibration

1. For force calibration, prepare a flow cell containing torsionally free DNA tethers. Preferably, the tethers are relatively long with respect to the magnetic bead size (*see* **Note 39**). Start the measurements with the magnets far away, exerting negligible force. Move the magnets quickly down to the position that needs to be calibrated, keep the magnets fixed for 120 s (*see* **Note 40**), and move the magnets upwards. Append two stretches of negligible force before and after the experiment to provide a reference for drift correction. If possible, increase the sample rate f_s of the camera to minimize motion blurring. Perform multiple calibration measurements at different magnet positions (*see* **Note 39**).
2. Load the data into data analysis software such as LabVIEW, Origin, Python, or Excel. Correct the drift by subtracting a term proportional with time from the extension prior to further analysis (*see* **Note 41**).
3. Exclude anomalous events, such as sticking (*see* **Note 42**), double bead attachment to a single tether (*see* **Note 43**), or double tether attachment to a single bead (*see* **Note 44**).
4. Evaluate the *X*-coordinates (the direction of the magnetic field) in the time domain where the magnet was exerting a constant force. Compute the single-sided power spectral density (PSD) in units of $\mu m^2_{rms}/Hz$.
5. Exclude all spectral components below 1 Hz, to discard $1/f$ noise and to minimize the effect of drift.
6. Fit the PDS to a blur and aliasing corrected PSD function to obtain the cutoff frequency to calculate the force:

$$PDS_{corrected}(f, f_c) = \frac{\sigma^2}{f_s} + \sum_{n=-1}^{1} \frac{k_B T}{\gamma \pi^2 (f_c^2 + (f + n f_s)^2)} \left(\frac{sin(W\pi(f + n f_s))}{W\pi(f + n f_s)} \right) \quad (1)$$

   See **Note 45** for a derivation of Eq. 1 and a full description of the parameters.
7. Plot the force as a function of magnet position h, and fit the data with a bi-exponential decay [31].

$$F(h) = F_{max}\left(\alpha e^{\frac{-h}{h_1}} + (1-\alpha) e^{\frac{-h}{h_2}}\right) \quad (2)$$

   This relation is unique for each combination of magnets and the type of magnetic beads. For our setup and 2.8 μm beads, we obtained $F_{max} = 85$ pN, $\alpha = 0.7$, $h_1 = 1.4$ mm, and $h_2 = 0.8$ mm.

3.8 Force Spectroscopy Experiments

1. For a dynamic force spectroscopy experiment on a torsionally free substrate, move the magnets down, increasing the force, and subsequently upwards, releasing the force. Move the magnets at a speed of 0.2 mm/s (*see* **Note 46**). Minimize the dwell time at the highest force to reduce the chance of a tether break. Several variations in trajectories are found in **Note 47**. Optionally, two stretches of low force can be appended before and after the experiment for drift correction.
2. For a dynamic force spectroscopy experiment on a torsionally constrained substrate, follow the same procedure as above. Optionally, pre-twist the torsionally constrained substrate before a dynamic force spectroscopy experiment: rotate the magnetic field while the stretching force upon the tether is kept low. Forces as low as 0.05 pN are sufficient for the bead to follow the rotation of the magnetic field. Rotate the magnets with a speed of two rotations per second (*see* **Note 48**).

3.9 Rotational Spectroscopy Experiments

1. For rotational spectroscopy on a torsionally constrained substrate, set the force by fixing the magnet height throughout the experiment. Rotate the magnets with a speed of two rotations per second. Apply positive twist as desired and relax the tether. Minimize the dwell time at the highest number of rotations (*see* **Note 49**). Apply an equal amount of negative twist at the same rotational speed and relax the tether. Optionally, two stretches with fixed rotation can be appended before and after the experiment for drift correction.

3.10 Data Analysis of Force Spectroscopy Experiments

1. Load the data into data analysis software such as LabVIEW, Origin, Python, or Excel. Calculate force from magnet height using Eq. 2. Correct the drift by subtracting a term proportional with time from the extension, such that the parts of the extension trace that were appended to the start and the end have the same height (*see* **Note 41**). Alternatively, a (linear) time-dependent term can be included in the fitting model. Plot the force as function of extension (*see* **Note 50**).
2. Exclude anomalous events, such as sticking (*see* **Note 42**), double bead attachment to a single tether (*see* **Note 43**), or double tether attachment to a single bead (*see* **Note 44**).
3. Fit the data.
   (a) For bare DNA, fit an extensible WLC model to the data:

$$z(F,t) = L\left(1 - \frac{1}{2}\sqrt{\frac{k_B T}{FP}} + \frac{F}{S}\right) + z_0 + dt \qquad (3)$$

where z is the extension, L is the contour length, P is the persistence length, F is the force, S is the stretch modulus,

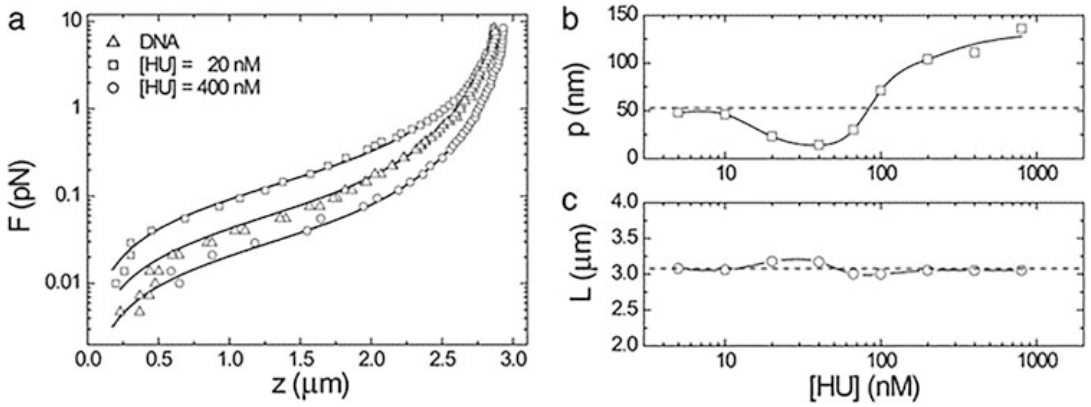

Fig. 3 The concentration of nucleoid-associated protein HU has a dual effect on the measured stiffness of a DNA tether. (**a**) The force–extension curves of DNA incubated with increasing concentration of HU. Solid lines represent fits to the WLC model (Eq. 3). The experiments reveal tether softening at nM HU concentration and tether stiffening at μM HU concentration. Experiments were performed in 60 mM of KCl and 20 mM HEPES (pH 7.9). (**b**, **c**) Persistence length and contour length as a function of HU concentration. The dashed lines represent bare DNA. Individual HU dimers introduce kinks in the DNA at nM HU concentration [59], resulting in a reduced persistence length. A rigid nucleoprotein filament is formed at high HU concentration. HU does not change the contour length. (Reproduced from ref. [10] with permission from PNAS (Copyright (2004) National Academy of Sciences, USA))

k_B is Boltzmann's constant, T is the absolute temperature, and z_0 is an offset in extension (*see* **Note 51**). Optionally, a drift, comprising amplitude d and time t, can be included.

(b) For (bacterial) chromatin, fit appropriate models to the data. Generally, the effect of protein binding can be captured in a modified WLC model by adjusting fitting parameters (*see* **Note 52**). An example is shown in Fig. 3, reproduced from Van Noort et al. [11], where the effect of HU binding on the mechanical parameters of a DNA tether is shown. Analysis of partial nucleoprotein filaments can be performed when the mechanical parameters of homogeneous, fully saturated nucleoprotein filaments have been established. Then, changes in extension can be described as a linear combination of the extensions of parts of bare DNA and parts of nucleoprotein filament [14, 41]. An example of a complex, dynamic chromatin structure is plotted in Fig. 4, showing force spectroscopy on a nucleosomal array reconstituted from tandem repeats of the *Widom* 601 sequence and eukaryotic histone proteins [42] (*see* **Note 53**).

(c) For archaeal chromatin composed of histone proteins, the model is more complicated. Archaeal histones have been shown to wrap DNA "endlessly" around stacked histone dimers into a so-called hypernucleosome [43]. Henneman et al. devised a statistical physics model to describe

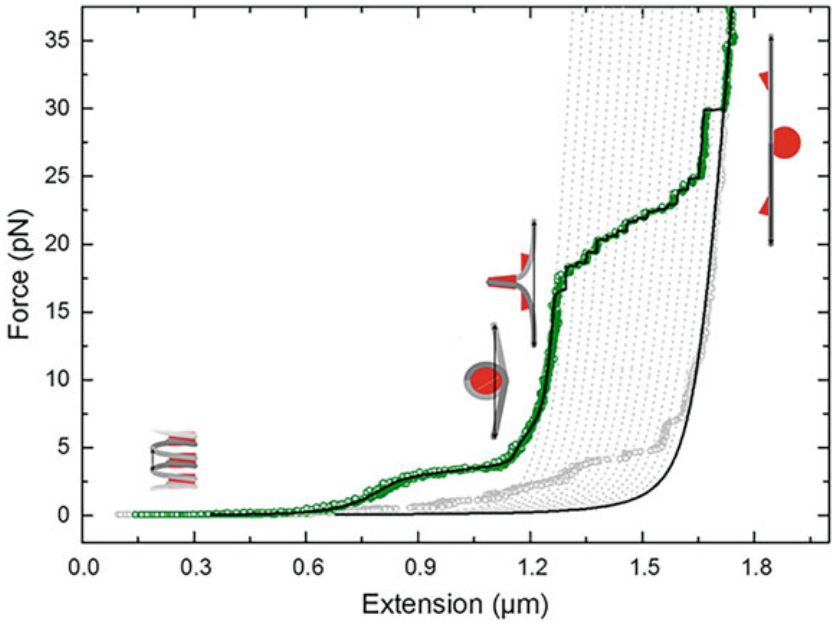

Fig. 4 Force spectroscopy on a eukaryotic chromatin fiber reveals different levels of compaction in 2 mM $MgCl_2$. The green curve is the stretch curve; the gray curve is the release curve. The black line describes a fit of the data to the statistical mechanics model [15]. The chromatin was reconstituted on an array of 15 Widom 601 nucleosome positioning sequences spaced by 50 base pairs [41]. The low-force regime shows a noncooperative transition at 3.5 pN, typical for a solenoid chromatin fiber, where the interactions between the nucleosomes are broken and the outer turn of DNA unwraps from the histone core, forming a beads-on-a-string structure. At approximately 6 pN, another transition takes place where this structure is slightly extended. Above 10 pN stepwise unwrapping indicates release of the final wrap of DNA from the histone core. The dashed lines represent discrete 25-nm steps. The chromatin fiber follows the force–extension curve of bare DNA at forces exceeding 25 pN and fits well with an extensible WLC model

hypernucleosome structure. This model takes into account three force-dependent conformations of the hypernucleosome (*see* Fig. 5c). In the first conformation, occurring at low force, the hypernucleosome is fully stacked, and all DNA is wrapped around the stack of histones. In the low force regime the hypernucleosome behaves as a Hookean spring which we model by a freely jointed chain (FJC) as described by Eq. 4:

$$z_{FJC}(F) = L_{dimer}\left(\coth\frac{Fb}{k_BT} - \frac{k_BT}{Fb}\right) \tag{4}$$

where Z_{FJC} is the extension per dimer, L_{dimer} represents the height of a single dimer, F the applied force, b the Kuhn length, k_{B} Boltzmann's constant and T the

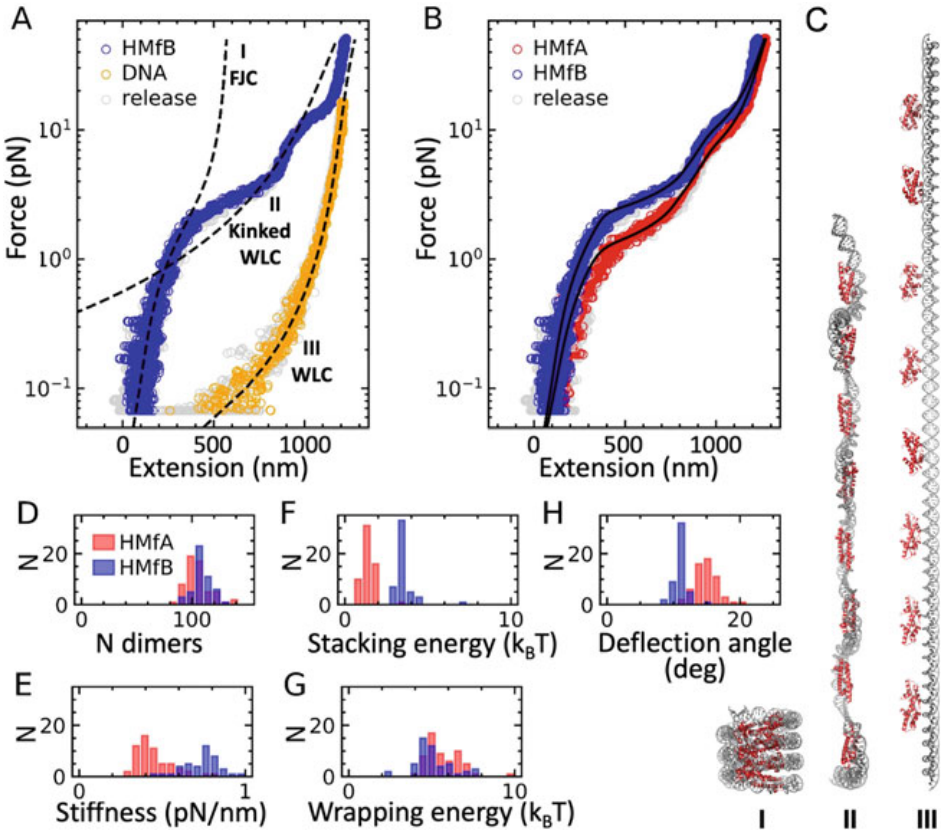

Fig. 5 Force spectroscopy on archaeal hypernucleosomes. (**a**) A typical force–extension curve of a hypernucleosome structure formed upon binding to DNA of *M. fervidus* histone B (HMfB) is shown in blue. The retraction curve (in gray) overlaps with the extraction curve. The absence of hysteresis implies that the histone dimers do not dissociate from the DNA. The force–extension curve of bare DNA (yellow) follows the characteristic wormlike chain model. (**b**) The HMfA homologue (red) has reduced stacking interactions as compared to HMfB (blue), as apparent from the lowered force plateau. Black lines indicate the fit to a statistical mechanics model that captures the transition between three conformations displayed in (**c**). At low force, histone dimers fold into a hypernucleosome (I) At several pN, the stacking interactions are disrupted; the wrapping of DNA onto the dimers results in a kinked DNA conformation (II). When the force exceeds 15 pN, part of the DNA unwraps from the dimers resulting in an unperturbed DNA trajectory (III). (**d**–**h**) Distribution of fit parameters obtained from >40 different fibers. Compared to protein–DNA complexes with HMfB, HMfA–DNA complexes exhibit a smaller stacking energy, a lower stiffness, but a larger deflection angle of the wrapped dimers

temperature. At low force the FJC model follows a Hookean spring, with a stiffness that is inversely proportional to the effective Kuhn length. At high forces the FJC model converges to an asymptote (*see* Fig. 5a), but in this range the hypernucleosome assumes another conformation, as described below, and in practice the model is only applied in the linear range. In the second conformation, at mid-force ranges, the chromatin fiber can be described with a beads-on-a-string model. In this conformation the DNA is still wrapped around histone dimers,

but the histone dimers do not interact, and the column of histone proteins is distorted. This conformation can be modeled as an extensible wormlike chain (eWLC) described by the equation below:

$$z_{WLC}(F) = L\left(1 - \frac{1}{2}\sqrt{\frac{k_B T}{FP}} + \frac{F}{S}\right) \tag{5}$$

where Z_{WLC} is the extension of the histone–DNA dimer complex, L is the contour length of the DNA in this complex, S is the stretch modulus of DNA, F is the force, T is the temperature, and P is the persistence length of DNA. The eWLC chain is commonly used to describe the behavior of bare DNA. In case of DNA-bound proteins, the trajectory of the DNA may include kinks. In that case the eWLC chain model still holds. However, just like in the previous section (Subheading 3.10, **step 3(b)**), a modified WLC model with adjusted fitting parameters is necessary (*see* **Note 52**). In particular, the effective persistence length of the DNA–histone complex is reduced. With N histone dimer-induced bends, the apparent persistence length P_{app} is

$$P_{app} = \frac{P}{1 + 8N^2 P(1 - \cos\frac{\alpha}{4}/L)^2} \tag{6}$$

where α is the protein-induced deflection angle of the DNA.

A third conformation exists at relatively high forces when part of the histone-bound DNA unwraps. In this conformation the histones are still bound to the DNA but do not deform it, resulting in a straight conformation where DNA is following the eWLC model as described before in Eq. 5.

From the force–extension models of each conformational state, the force-dependent free energy of each conformation can be calculated:

$$G_{FJC}(F) = \int z_{FJC}(F)dF - \mathcal{g}_{stack} - \mathcal{g}_{wrap} \tag{7}$$

$$= L_{dimer}\frac{k_B T}{b}\left(ln\left(\sinh\frac{Fb}{k_B T} - ln\left(\frac{Fb}{k_B T}\right)\right)\right) - \mathcal{g}_{stack} - \mathcal{g}_{wrap} \tag{8}$$

$$G_{WLC}(F) = \int z_{WLC}(F)dF - \mathcal{g}_{wrap} = L\left(F - \sqrt{\frac{Fk_B T}{P}} + \frac{F^2}{2S}\right) - \mathcal{g}_{wrap} \tag{9}$$

Here $\mathcal{g}_{\mathrm{stack}}$ and $\mathcal{g}_{\mathrm{wrap}}$ represent the protein–protein interaction energy and protein–DNA interaction energy,

respectively. In case of the straight conformational state, g_{wrap} is equal to 0.

The total free energy of the chromatin fiber in the magnetic tweezers is then obtained by summing the free energy contributions of each histone dimer in the hypernucleosome and subtracting the work performed by the bead $W(F)$:

$$G_{total} = G_{FJC} + G_{WLC} - W(F) \tag{10}$$

The extension of the HMf–DNA complex is then calculated as the Boltzmann-weighted mean extension:

$$< z_{total}(F) > = \frac{\sum_j z_j(F) e^{-G_j(F)/k_B T}}{\sum_j e^{-G_j(F)/k_B T}} + z_0 \tag{11}$$

in which an arbitrary offset z_0 accounts for the precise location of the DNA attachment to the bead (*see* **Note 51**).

Fitting Eq. 11 to the magnetic tweezers data, we are able to quantify the number of bound dimers, the stacking energy, the deflection angle, the stiffness of the hypernucleosome, and the wrapping energy (*see* Fig. 5d–h).

3.11 Data Analysis of Rotational Spectroscopy Experiments

1. Load the data into data analysis software. Correct the drift following the same procedure as that of the force spectroscopy experiments. Correct the offset in Z by computing the first percentile of the extension as a measurement of the surface and subtract it from all Z-coordinates. Calculate linking number density from magnet rotation (*see* **Note 54**). Plot the relative extension as a function of linking number density.
2. Exclude disruptive events, following the same procedure as that of the force spectroscopy experiments (*see* **Notes 55–58**).
3. Fit the data.
   (a) For bare DNA, a three-state model [37] describes the coexistence of twisted, melted, and plectonemic conformational states (*see* **Note 59**). An example is shown in Fig. 6.
   (b) For (bacterial) chromatin, an appropriate model to the data needs to be composed in which the torsional response of chromatin fibers should be modeled as a linear combination of twisted and wrapped DNA [44] (*see* **Note 60**).

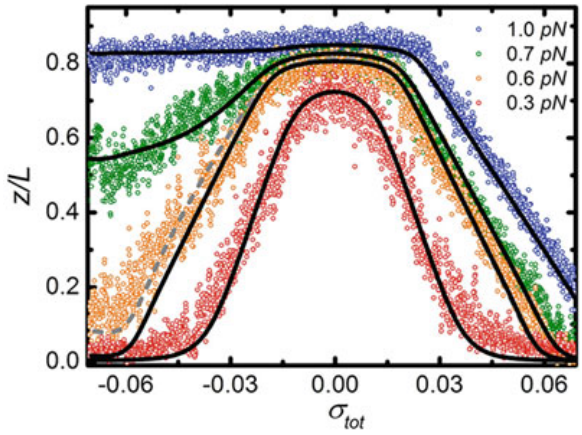

Fig. 6 The relative extension of a DNA tether as a function of linking number density shows an asymmetric response to twist at forces above 0.5 pN. At low force, plectonemes are formed for both negative and positive twists, reducing the measured extension. Negative twist induces DNA melting at higher force, which keeps the extension constant. The lines represent calculated extensions following a three-state model that distributes twisted, plectonemic, and melted regions in the DNA. (Reproduced from ref. [36] with permission from Elsevier)

4 Notes

1. Although the torque is proportional to the strength of the magnetic field, the force in MT is proportional to the gradient of the magnetic field and, therefore, rapidly reduces with distance.
2. In the measurement buffer, HEPES sets the pH and NaCl the ionic strength. TWEEN 20 is a detergent and prevents aggregation of proteins. Sodium azide is highly toxic and is added to prevent bacterial growth. When sodium azide is omitted, use sterile solutions or replace buffers frequently. BSA is used as a crowding agent and retains flow cell passivation. In the passivation buffer, a high concentration of BSA is used to block nonspecific binding of DNA and beads and tethers to the surface.
3. For the DNA tethers, we generally use a pUC18-based DNA plasmid, carrying ampicillin resistance. We digest this plasmid with restriction enzymes BsaI and BseYI. For the handles of the torsionally constrained construct, we also use a pUC18 DNA plasmid as a template for PCR. The forward and backward primers are 5′ CTC CAA GCT GGG CTG TGT 3′ and 5′ GAT AAA TCT GGA GCC GGT GA 3′. Reconstitution of chromatin fibers, as shown in Fig. 4, was done using a plasmid containing 15 repeats of the *Widom* 601 positioning sequence spaced by 50 base pairs [42].

4. Make LB medium by diluting 10-g tryptone, 10-g NaCl, and 5-g yeast extract in 1000-mL Milli-Q water. Make LB agar plates by diluting 10-g tryptone, 10-g NaCl, 5-g yeast extract, and 20-g agar in 1000-mL Milli-Q water.
5. We advise to use Invitrogen Dynabeads™ M-270 Streptavidin or MyOne™ Streptavidin T1 paramagnetic beads. These beads have a relatively high iron content (MyOne: 26%/M-270: 14%) and monodispersed size distribution (CV $<$ 3%), which is important for reaching high forces and reliable bead tracking and force calibration.
6. When handling frozen competent cells, it is important to keep them cool. Frozen cells are very sensitive to temperature and will lose competence if not kept on ice.
7. Very low concentrations, down to picograms per microliter, are sufficient.
8. Use a reaction volume of at least 20–50 μL/μg DNA in a digestion.
9. Digestion of (hundreds of) micrograms of DNA plasmid requires overnight incubation. We frequently observe undigested DNA plasmid in agarose gel electrophoresis if we shorten the incubation time.
10. Inactivation temperatures vary for different restriction enzymes.
11. The Promega Wizard SV Gel and PCR cleanup kit uses high concentrations of chaotropic agents to perturb the hydrogen bond network of the solvent, enabling DNA to bind to the silica of the cleanup kit [45–48].
12. Multiple elutions with the spin column improve the yield. Furthermore, a longer incubation time increases the yield. For precious samples, the increased yield outweighs the increased waiting time.
13. This step can be performed longer, up to overnight.
14. Keep the reaction volumes small to reduce cost.
15. The difference between dNTP and ddNTP is that the ddNTP is lacking an OH group at its 3′ carbon, which is required for DNA polymerization. It prevents incorporation of more than one affinity tag per DNA strand as the strand cannot be extended.
16. Ethidium bromide and GelRed are intercalating agents that fluoresces upon binding to DNA and illumination by a UV light source [49]. To visualize DNA in agarose gels, it can be added to the electrophoresis gel or to the running buffer.
17. If there is aspecific binding of the primers, the percentage of DMSO can be further increased. If the addition of more

DMSO does not solve the problem, it is necessary to redesign the primers.

18. DpnI cleaves methylated sites. Plasmids propagated in and purified from *E. coli* generally contain methylation on GTAC sites.
19. Minimize UV exposure of the sample to prevent DNA damage. Accordingly, block UV exposure of the gel with a nontransparent material such as aluminum foil. Use flanking DNA ladders to estimate the position to cut the DNA fragment from the gel. After cutting, verify that the desired band is cut out by imaging on the UV transilluminator.
20. Dissolving the gel generally results in milliliters of DNA solution. To purify, load the spin column several times. Do not exceed the maximum amount of DNA that can be purified as specified for the column.
21. BseYI can remain bound to DNA after digestion and alter the migration of DNA in agarose gels. To dissociate BseYI, add SDS to a final concentration of 0.5% or purify DNA before agarose gel electrophoresis, for instance, with the Promega Wizard SV Gel and PCR cleanup kit.
22. DNA plasmid pUC18 was used as a template for the primers to construct DNA handles.
23. The PCR mixture contains 10% of biotin or digoxigenin labeled dUTP. The PCR product will thus have approximately 10–20 affinity tags incorporated.
24. Use labeled dUTPs instead of ddUTPs, since chain termination is undesired.
25. The small digestion products from the ends of the DNA (7 base pairs on the *BseYI*-side and 32 base pairs on the *BsaI*-side) are discarded by the Promega Wizard SV Gel and PCR cleanup kit, which has a cutoff at 100 base pairs.
26. The digested pUC18 DNA (with 601-array) is approximately seven times the length of the digested PCR products. To reach the approximate 1:1:1 molar ratio, use 1:7:1 weight ratio (multi-digoxigenin PCR product/digested pUC18 DNA (with 601-array)/multi-biotin PCR product).
27. The unit definition of T4 DNA ligase can be quite ambiguous. In our protocol, we use excess amounts of T4 ligase for optimal yields.
28. Purifying a DNA construct with multiple affinity tags will strongly reduce the yield as the affinity tags increase DNA adhesion to the column. The yield can be improved by multiple elutions and longer incubation times (up to hours).

29. Nitrocellulose coating of the coverslip makes the surface hydrophobic, enhancing anti-digoxigenin binding.
30. During flushing, turn the flow cell upside down such that unbound beads will detach from the surface.
31. Incubate the flow cell with a high concentration of BSA to passivate the surface area. This step will reduce sticking of chromatin tethers during experiments.
32. DNA can be replaced by preincubated protein–DNA complexes, for instance, reconstituted or native chromatin.
33. During incubation of paramagnetic beads, keep the flow cell upright such that the beads move toward the coated coverslip by gravity.
34. Our MT setup, depicted in Fig. 2, is home built and equipped with custom control and tracking software written in LabVIEW (available upon request) [21]. A pair of magnets are mounted 0.8 mm apart, at the center axis of a hollow shaft stepper motor that is mounted on a stepper motor-actuated translation stage. The magnets are oriented with their magnetization axis vertically, in opposite directions. For proper orientation, ensure that the magnets attract each other yet do not allow rotation around the axis connecting the centers of the magnets. The microscope objective is mounted on a stepper motor-actuated translation stage to allow for coarse focusing. Stepper motors are controlled by a six-axis two-phase stepper motor driver. A collimated LED is mounted in a kinematic pitch/yaw adapter above the hollow shaft motor and provides a homogeneous illumination of the flow cell. We use an inverted microscope layout, including a tube lens and monochrome camera, to record the out-of-focus images of the Lorentz–Mie scattering pattern of the tethered bead [50]. The flow cell is mounted on a XYZ piezo stage, for accurate control of the focus position. The XYZ piezo stage is mounted onto an XY positioning stage, for manual coarse translation of the flow cell. The microscope setup is surrounded by a box to minimize acoustic and thermal fluctuations and to protect the setup from dust.
35. Before each experiment, the focus should be adjusted so that we always measure in the same plane.
36. An automatic bead finder algorithm is currently implemented, which cross-correlates the field of view with a computer-generated reference image which resembles the beads. Beads are selected by setting a threshold on the cross-correlation amplitude.
37. During a typical measurement, a series of frames are acquired and processed in real time. The magnet position and rotation

are recorded in synchrony by the same software that controls the frame grabber. Data collection is buffered in two parallel processes:

(a) Image acquisition

The camera captures full frames at a speed of 30 fps. The assigned ROIs and frame numbers are extracted and stored in a buffer.

(b) Image analysis

In parallel, the buffer is read out and analyzed. Each ROI is cross-correlated with a set of computer-generated reference images, using an FFT-based correlation algorithm. The maximum of the cross-correlation represents the center of the bead and is determined with sub-pixel accuracy. The phase of the cross-correlation at this location is also extracted, converted to a *Z*-coordinate and written into a binary file. From the frame number and frame rate, a time column is computed and stored in the same file [21].

After each measurement, the binary file is transformed into an ASCII file that allows for versatile data processing. This file contains a time column, a column with the motor positions, and four columns per bead: three spatial coordinates and the amplitude of the cross-correlation.

38. Any appropriate bead tracking algorithm will suffice for this step. Use, for instance, the cross-correlation method [51], a center-of-mass calculation [52], directly fitting a Gaussian curve to the intensity profile [53], the quadrant interpolation method [54], or the phase tracking method [21].
39. We used a 6955 base pairs DNA tether (≈ 2.4 μm) to calibrate 1.0 and 2.8 μm diameter magnetic beads and recorded images with a frame rate of 200 Hz. Longer tethers provide a better signal-to-noise ratio; therefore, it is not uncommon that Lambda-DNA is used for calibration, which is 48,502 base pairs (≈ 16.5 μm) in length. If appropriate camera corrections are applied (i.e., motion blur and aliasing, *see* **Notes 43–45**), force calibration can be performed with shorter tethers.
40. The required measurement time τ_m for a desired statistical accuracy ε is described in Eqs. 12 and 13 [31]:

$$\tau_m \approx \frac{12\pi^2\eta RL}{f\varepsilon^2} \text{ for } F > 1 \text{ pN}; \tag{12}$$

$$\tau_m \approx \frac{8\pi^2\eta RPL}{k_B T\varepsilon^2} \text{ for } F < 1 \text{ pN}, \tag{13}$$

where η is the viscosity of water, R is the radius of the bead, L is the DNA contour length, F is the calibrated force, and P is the

DNA persistence length. Typically, the statistical accuracy ε is set to 0.05. We measure each magnet position for 120 s, which is well within limits.

41. A plot of extension as a function of time may reveal drift as a steady increase or decrease of extension over time. When beginning and ending a trajectory at low force (or no rotations), at which the *Z*-position of the bead is constrained by the bottom slide of the flow cell, compare the first percentile of the bead height of these two segments to quantify the drift. Calculate the first percentile rather than the average, since the surface poses a one-sided boundary to the bead motion. The first percentile will give a good estimation of the surface position, which is required for drift characterization. Typically, we measure less than 1 nm/s drift of the extension, yet this can accumulate to significant deviations of the measured force–extension curves.
42. When the bead is in close proximity to the surface, nonspecific interactions between the bead and the surface can cause the bead or part of the tether to stick to the flow cell bottom, immobilizing the bead. Small forces are generally sufficient to unstick the bead and resume the measurement as normal. As opposed to intramolecular rupturing or folding events, (un)sticking events can be identified in the data as an abrupt step in the coordinates in three dimensions, rather than only in the *Z*-direction.
43. A double bead doubles the force exerted on the tether. Therefore, transitions are measured at half the force at which they are expected (for instance, DNA overstretching measured at half the force). The measured persistence length is double of that measured with a single bead. Furthermore, the data is generally very noisy, since tracking becomes problematic with two beads in the same ROI.
44. A double tether halves the force exerted on the tether. Therefore, transitions are measured at double the force as they are expected and add up (for instance, double the amount of stepwise unwrapping events when stretching chromatin, measured at double the force). The measured persistence length is half that of a single tether. A plot of the *X*- versus *Y*-coordinates of the bead during drift characterization is asymmetric.
45. The magnetic force pulls the tethered bead in the *Z*-direction and is counteracted by a restoring force from the tether. Brownian motion causes the bead to move away from its central position. The potential energy $E_p(x)$ in the direction of the field (*X*-direction) around the equilibrium position is described by

$$E_p(x) = \frac{1}{2} k_x \delta x^2 \tag{14}$$

where δx^2 is the variance of the bead fluctuations. The effective trap stiffness k_x follows

$$k_x = \frac{F}{z} \tag{15}$$

where F is the stretching force and z is the bead height. The equipartition theorem states that the energy per degree of freedom equals $\frac{1}{2} k_B T$. The force therefore follows

$$F = \frac{k_B T z}{< \delta x^2 >} \tag{16}$$

For an accurate experimental determination of the force, however, it is necessary to look into the frequency dependence of the thermal fluctuations of x. Start by computing the PSD in the direction of the field at constant force. Since the PDS follows a Lorentzian curve

$$PDS_{termal}(f, f_c) = \frac{k_B T}{\gamma \pi^2 (f_c^2 + f^2)} \tag{17}$$

it is fully defined by the lateral friction coefficient γ and the cut-off frequency f_c

$$f_c = \frac{k_x}{2\pi\gamma} \tag{18}$$

The friction coefficient depends on the bead radius R and the viscosity η (which increases with closer proximity to the surface; *see* **Note 61**):

$$\gamma = 6\pi\eta R \tag{19}$$

leading together with Eq. 15 to

$$F = 12\pi^2 \eta R z f_c \tag{20}$$

Thus fitting the cutoff frequency from the PDS yields the force for a given magnet position. However, the finite integration time of the camera averages out some of the bead's movement, an effect known as blurring. To account for blurring, a correction term C_{blur} must be applied [30–32, 55, 56]:

$$C_{blur} = \left(\frac{\sin(W\pi f)}{W\pi f} \right)^2 \tag{21}$$

where W is the frame integration time. The finite sampling frequency of the camera causes another artifact, known as aliasing. Aliasing can be described by folding back the parts of the spectrum that exceed the sampling frequency f_s:

$$PDS_{alias}(f,f_c) = \sum_n PDS_{thermal}(f + nf_s,f_c) \cdot C_{blur}(f + nf_s,f_c) \tag{22}$$

It is usually sufficient to include only one aliasing term, i.e., $n = -1 \ldots 1$ [30]. Finally, the PSD is offset by a tracking error of variance σ^2 that is independent of frequency [56]:

$$PDS_{tracking} = \frac{\sigma^2}{f_s} \tag{23}$$

in which f_s is the sampling frequency. Overall, fitting

$$PDS_{corrected}(f,f_c) = \frac{\sigma^2}{f_s} + \sum_{n=-1}^{1} \frac{k_B T}{\gamma \pi^2 (f_c^2 + (f + nf_s)^2)} \left(\frac{\sin(W\pi(f + nfs))}{W\pi(f + nfs)} \right)^2 \tag{24}$$

to the experimental spectrum of the lateral fluctuations will yield the cutoff frequency which is used to calculate the force.

46. The loading rate increases exponentially with magnet speed. For forces below 5 pN, we typically have a loading rate that ranges between 0 and 0.75 pN/s. High loading rates reduce the rate of nonequilibrium events as demonstrated by studying the breaking of bonds between antibodies [57].
47. Several variations of magnet trajectories can be used:
    (a) Repeat loops to gain insight into the reversibility of DNA folding.
    (b) To approach a linear loading rate, break up the trajectory in several segments with decreasing magnet speeds.
    (c) Start with a short force ramp up to 0.5 pN to set free loosely stuck beads.
48. Torsionally constrained substrates build up torque while stretched and consequently respond differently to force. These substrates can be pre-twisted before an experiment to study the role of supercoiling. DNA compacted by a protein like HU, for instance, has an intrinsically twisted structure.
49. Supercoiling reduces the bead height, which increases the probability of beads or tethers to stick to the surface. Minimizing the dwell time at the maximum number of rotations reduces sticking.
50. Plot force as function of extension. Plotting it in this way is customary for optical tweezers and allows for easy comparison between methods. Because MT forms a force clamp rather than a position clamp, this way of plotting may be counterintuitive.
51. For tethers with a length that is in range with the size of the bead, off-center attachment of the DNA to the bead may lead to a large error in the measured extension. Superparamagnetic beads have a small but finite permanent magnetic moment,

giving them a preferred orientation when exposed to a magnetic field [58]. Since tethering happens in the absence of the magnetic field, application of force will turn the magnetic moment in the direction of the magnetic field, typically horizontally, while maximizing the height of the bead. When the DNA is attached at a location exactly at the circumference of the bead that has equal distance between the magnetic poles, it will rotate the bead, such that the attachment point will be at the bottom of the bead. Any location remote from this circle will still rotate the bead around the horizontal axis along the poles but cannot spin the bead along the horizontal axis perpendicular to the poles. Consequently, there will be an offset between the height of the bead and the extension of the tether, and the measured extension is underestimated. This artifact is specific for MT and can be corrected by shifting the data in the *Z*-direction or by including this offset as a fitting parameter.

52. Specific modes of protein binding yield distinctive patterns:
    (a) Coating the DNA tether yields a stiffening of the DNA, which can be parameterized by an increased persistence length in the entropic regime at low force and/or an increased stretch modulus at high force. These two effects can only be differentiated when a large force range is probed. Examples are HU (at μM concentration) [11] and H-NS (at nM concentration) [14, 59, 60].
    (b) Bending induces a kink in the DNA trajectory, which is apparent as a reduced persistence length [61]. The magnitude of this reduction scales with the kink angle and the number of kinks, which reflect the structure and number of proteins bound to the tether. Examples of chromatin proteins that introduce a kink are HU (at nM concentration) [11, 62] and IHF (at nM concentration) [63].
    (c) Wrapping of DNA around proteins results in both a reduction of the persistence length, similar to bending, and a reduction of the contour length. When exactly one wrap is formed, the persistence length is similar to that of bare DNA. The archetype of wrapping proteins is the eukaryotic histone octamer that wraps 1.7 turns of DNA [64–66]. Archaeal histones can wrap smaller DNA lengths or larger DNA lengths, when organized into a hypernucleosome [67, 68].
    (d) Bridging involves protein-induced formation of contacts between distant part of the DNA tether and results in a large reduction of the contour length. The DNA that is captured in the loop does not contribute to the extension of the tether. An example of a DNA bridging protein is H-NS, whose mode of binding depends on the concentration of monovalent and divalent ions [14, 59, 60].

(e) Melting parts of the dsDNA tether by force and or torque yields sections of single-stranded DNA. This leads to a 1.6 times extension of the contour length, as well as a reduction of the persistence length down to a few nanometers in absence of protein covering the single-strand DNA [42]. Single-strand binding proteins like SSB prevent annealing of force induced, melted DNA, yielding force–extension curves that display a large hysteresis [69].

53. Various force regimes reveal different conformations of eukaryotic chromatin that can all be captured in a force-dependent linear combination of bare DNA and four different nucleosome structures [16]. Bacterial chromatin typically consists of proteins that bend, rather than wrap DNA, have a smaller footprint, and are usually interspersed with different types of proteins. Furthermore, they may have more varying sequence preferences. Nevertheless, a similar analysis, customized for different characteristics of individual proteins, can be used to retrieve a detailed understanding of chromatin folding based on force spectroscopy. When the chromatin conformation is not stable due to changes of protein concentration, force, or salt, this may result in a change in extension. From such changes it is possible to extract binding and/or dissociation rates.
54. Calculate the linking number density, using $\sigma = \Delta Lk/Lk_0$, where Lk_0 is the linking number of DNA. Lk_0 equals the contour length in base pairs divided by the helical pitch of DNA, which is 10.4 base pairs. The change in linking number, ΔLk, equals the number of rotations of the magnets.
55. A double bead affects rotational spectroscopy measurements similar to force spectroscopy measurements. The tether is more likely to break since the force that is kept constant during the measurement is double of that expected.
56. A double tether affects rotational spectroscopy measurements similar to force spectroscopy measurements. Double tethers can easily be identified when twisting the tether. During the first turn, the bead is pulled down by a large step, as the two molecules get braided. Subsequent twist lowers the bead for both negative and positive rotations, as opposed to single tethers, for which the extension is independent of negative twist at forces exceeding 1 pN.
57. The DNA tether can become nicked during sample preparation. A single nick is sufficient to release torque, and consequently the tether cannot be used for rotational spectroscopy. These tethers can be discarded during an initial rotation experiment or can serve as control for torsionally unconstraint tethers.

58. Plot all X-coordinates versus all Y-coordinates during rotation of the bead. The shape of this plot should be a circle. The radius of the circle equals the attachment offset from the center of the bead, from which the vertical offset can be calculated.
59. Since mechanical properties of twisted DNA are much more complex than those of torsionally free DNA, fitting the curves is challenging. The three-state model developed by Meng et al. [37] describes the coexistence of twisted, melted, and plectonemic conformational states. The data and the model feature symmetric buckling at low forces ($f < 0.6$ pN), where both positive and negative twists are absorbed by plectonemes. At higher forces ($f > 0.6$ pN) the extension–twist curve becomes asymmetric, and negative twist is absorbed by local melting of the DNA.
60. Quantitative analysis of the torsional stress in chromatin filaments is more involved. Bending proteins (such as HU of IHF) and wrapping proteins (such as HMf or eukaryotic histones) induce writhe in a torsionally constrained tether, while twist remains constant. The torsional stiffness of such fibers has not been measured, though quantification is highly desirable to test proposed models of twist-induced (de)compaction of chromatin fibers and their role in transcription regulation. Eukaryotic tetrasomes have been shown to have a complex dynamic chirality [34, 35].
61. Beads experience an increasing viscosity as the distance to the surface approaches the bead diameter [70]. The height dependence of the lateral friction coefficient γ is approximated by Faxén's law:

$$\gamma = \frac{\gamma_0}{1 - \frac{9R}{16h} + \frac{R^3}{8h^3} - \frac{45R^4}{256h^4} - \frac{R^5}{16h^3}} \tag{25}$$

where $\gamma_0 = 6\pi\eta R$ is the bulk friction coefficient, η is the viscosity, R is the radius of the bead, and h is the distance of the bead center to the surface.

References

1. Hocher A, Laursen SP, Radford P et al (2023) Histone-organized chromatin in bacteria. Nat Microbiol 8(11):2006-2019. https://doi.org/10.1038/s41564-023-01492-x
2. Alva V, Lupas AN (2019) Histones predate the split between bacteria and archaea. Bioinformatics 35(14):2349–2353. https://doi.org/10.1093/bioinformatics/bty1000
3. Schwab S, Boyle AL, Dame RT (2023) Novel histones and histone variants families in prokaryotes. bioRxiv 2023.06.01.543357. https://doi.org/10.1101/2023.06.01543357
4. Hu Y, Deiss S, Joiner JD et al (2023) Atomic resolution structure of a DNA-binding histone protein from the bacterium *Bdellovibrio bacteriovorus*. bioRxiv 2023.02.26.530074. https://doi.org/10.1101/2023.02.26.530074
5. Hu Y, Schwab S, Deiss S et al (2024) Bacterial histone HBb grom *Bdellovibrio bacteriovorus*

compacts DNA by bending. Nucleic Acids Res https://doi.org/10.1093/nar/gkae485
6. Luijsterburg MS, White MF, Van Driel R, Dame RT (2008) The major architects of chromatin: architectural proteins in bacteria, archaea and eukaryotes. Crit Rev Biochem Mol Biol 43:393–418
7. Bustamante C, Bryant Z, Smith SB (2003) Ten years of tension: single-molecule DNA mechanics. Nature 421:423–427
8. Smith S, Finzi L, Bustamante C (1992) Direct mechanical measurements of the elasticity of single DNA molecules by using magnetic beads. Science (80-) 258:1122–1126
9. Strick TR, Allemand JF, Bensimon D et al (1996) The elasticity of a single supercoiled DNA molecule. Science 271:1835–1837
10. Gosse C, Croquette V (2002) Magnetic tweezers: micromanipulation and force measurement at the molecular level. Biophys J 82: 3314–3329
11. van Noort J, Verbrugge S, Goosen N et al (2004) Dual architectural roles of HU: formation of flexible hinges and rigid filaments. Proc Natl Acad Sci 101:6969–6974
12. van Loenhout MTJ, van der Heijden T, Kanaar R et al (2009) Dynamics of RecA filaments on single-stranded DNA. Nucleic Acids Res 37: 4089–4099
13. Lionnet T, Allemand JF, Revyakin A et al (2012) Single-molecule studies using magnetic traps. Cold Spring Harb Protoc 7:34–49
14. Lim CJ, Kenney LJ, Yan J (2014) Single-molecule studies on the mechanical interplay between DNA supercoiling and H-NS DNA architectural properties. Nucleic Acids Res 42: 8369–8378
15. Van Der Valk RA, Vreede J, Crémazy F, Dame RT (2014) Genomic looping: a key principle of chromatin organization. J Mol Microbiol Biotechnol 24:344–359
16. Meng H, Andresen K, Van Noort J (2015) Quantitative analysis of single-molecule force spectroscopy on folded chromatin fibers. Nucleic Acids Res 43:3578–3590
17. Yan J, Skoko D, Marko JF (2004) Near-field-magnetic-tweezer manipulation of single DNA molecules. Phys Rev E Stat Nonlinear Soft Matter Phys 70:011905
18. Berghuis BA, Köber M, van Laar T, Dekker NH (2016) High-throughput, high-force probing of DNA-protein interactions with magnetic tweezers. Methods 105:90–98
19. Ribeck N, Saleh OA (2008) Multiplexed single-molecule measurements with magnetic tweezers. Rev Sci Instrum 79:094301
20. De Vlaminck I, Henighan T, Van Loenhout MTJ et al (2011) Highly parallel magnetic tweezers by targeted DNA tethering. Nano Lett 11:5489–5493
21. Brouwer TB, Kaczmarczyk A, Van Noort J (2020) Multiplexed nanometric 3D tracking of microbeads using an FFT-phasor algorithm. Biophys J 118(9):2245–2257
22. Lipfert J, Wiggin M, Kerssemakers JWJ et al (2011) Freely orbiting magnetic tweezers to directly monitor changes in the twist of nucleic acids. Nat Commun 2:439
23. Lipfert J, Kerssemakers JWJ, Jager T, Dekker NH (2010) Magnetic torque tweezers: measuring torsional stiffness in DNA and RecA-DNA filaments. Nat Methods 7:977–980
24. Fisher JK, Cribb J, Desai KV et al (2006) Thin-foil magnetic force system for high-numerical-aperture microscopy. Rev Sci Instrum 77: nihms8302
25. Oliver PM, Park JS, Vezenov D (2011) Quantitative high-resolution sensing of DNA hybridization using magnetic tweezers with evanescent illumination. Nanoscale 3:581–591
26. Graham JS, Johnson RC, Marko JF (2011) Concentration-dependent exchange accelerates turnover of proteins bound to double-stranded DNA. Nucleic Acids Res 39:2249–2259
27. Graham JS, Johnson RC, Marko JF (2011) Counting proteins bound to a single DNA molecule. Biochem Biophys Res Commun 415:131–134
28. Long X, Parks JW, Bagshaw CR, Stone MD (2013) Mechanical unfolding of human telomere G-quadruplex DNA probed by integrated fluorescence and magnetic tweezers spectroscopy. Nucleic Acids Res 41:2746–2755
29. Vilfan ID, Lipfert J, Koster DA et al (2009) Magnetic tweezers for single-molecule experiments. In: Single-molecule biophysics. Springer, New York, pp 371–395
30. Te Velthuis AJW, Kerssemakers JWJ, Lipfert J, Dekker NH (2010) Quantitative guidelines for force calibration through spectral analysis of magnetic tweezers data. Biophys J 99:1292–1302
31. Yu Z, Dulin D, Cnossen J et al (2014) A force calibration standard for magnetic tweezers. Rev Sci Instrum 85(12):123114
32. Daldrop P, Brutzer H, Huhle A et al (2015) Extending the range for force calibration in magnetic tweezers. Biophys J 108:2550–2561
33. Gupta P, Zlatanova J, Tomschik M (2009) Nucleosome assembly depends on the torsion in the DNA molecule: a magnetic tweezers study. Biophys J 97:3150–3157

34. Vlijm R, Lee M, Lipfert J et al (2015) Nucleosome assembly dynamics involve spontaneous fluctuations in the handedness of tetrasomes. Cell Rep 10:216–225
35. Vlijm R, Lee M, Ordu O et al (2015) Comparing the assembly and handedness dynamics of (H3.3-H4)2 tetrasomes to canonical tetrasomes. PLoS One 10(10):e0141267
36. Kruithof M, Chien F, de Jager M, van Noort J (2008) Subpiconewton dynamic force spectroscopy using magnetic tweezers. Biophys J 94:2343–2348
37. Meng H, Bosman J, Van Der Heijden T, Van Noort J (2014) Coexistence of twisted, plectonemic, and melted DNA in small topological domains. Biophys J 106:1174–1181
38. Marko JF, Siggia ED (1995) Stretching DNA. Macromolecules 28:8759–8770
39. Bustamante C, Smith SB, Liphardt J, Smith D (2000) Single-molecule studies of DNA mechanics. Curr Opin Struct Biol 10:279–285
40. Marko JF (2007) Torque and dynamics of linking number relaxation in stretched supercoiled DNA. Phys Rev E Stat Nonlinear Soft Matter Phys 76:021926
41. Smith SB, Cui Y, Bustamante C (1996) Overstretching B-DNA: the elastic response of individual double-stranded and single-stranded DNA molecules. Science (80-) 271:795–798
42. Lowary P, Widom J (1998) New DNA sequence rules for high affinity binding to histone octamer and sequence-directed nucleosome positioning. J Mol Biol 276:19–42
43. Henneman B et al (2021) Mechanical and structural properties of archaeal hypernucleosomes. Nucleic Acids Res 49(8):4338–4349
44. Bancaud A, Wagner G, Conde e Silva N et al (2007) Nucleosome chiral transition under positive torsional stress in single chromatin fibers. Mol Cell 27:135–147
45. Chen CW, Thomas CA (1980) Recovery of DNA segments from agarose gels. Anal Biochem 101:339–341
46. Marko MA, Chipperfield R, Birnboim HC (1982) A procedure for the large-scale isolation of highly purified plasmid DNA using alkaline extraction and binding to glass powder. Anal Biochem 121:382–387
47. Boom R, Sol C, Salimans MMM et al (1990) Rapid and simple method for purification of nucleic acids. J Clin Microbiol 28:495–503
48. Salvi G, De Los Rios P, Vendruscolo M (2005) Effective interactions between chaotropic agents and proteins. Proteins Struct Funct Genet 61:492–499
49. LePecq JB, Paoletti C (1967) A fluorescent complex between ethidium bromide and nucleic acids. Physical-chemical characterization. J Mol Biol 27:87–106
50. Lee S-H, Roichman Y, Yi G-R et al (2007) Characterizing and tracking single colloidal particles with video holographic microscopy. Opt Express 15:18275
51. Gelles J, Schnapp BJ, Sheetz MP (1988) Tracking kinesin-driven movements with nanometre-scale precision. Nature 331:450–453
52. Lee GM, Ishihara A, Jacobson K (1991) Direct observation of brownian motion of lipids in a membrane. Proc Natl Acad Sci USA 88:6274–6278
53. Anderson CM, Georgiou GN, Morrison IE et al (1992) Tracking of cell surface receptors by fluorescence digital imaging microscopy using a charge-coupled device camera. Low-density lipoprotein and influenza virus receptor mobility at 4 degrees C. J Cell Sci 101(Pt 2):415–425
54. Van Loenhout MTJ, Kerssemakers JWJ, De Vlaminck I, Dekker C (2012) Non-bias-limited tracking of spherical particles, enabling nanometer resolution at low magnification. Biophys J 102:2362–2371
55. Wong WP, Halvorsen K (2006) The effect of integration time on fluctuation measurements: calibrating an optical trap in the presence of motion blur. Opt Express 14:12517–12531
56. van der Horst A, Forde NR (2010) Power spectral analysis for optical trap stiffness calibration from high-speed camera position detection with limited bandwidth. Opt Express 18: 7670–7677
57. Sitters G, Kamsma D, Thalhammer G et al (2014) Acoustic force spectroscopy. Nat Methods 12:47–50
58. Klaue D, Seidel R (2009) Torsional stiffness of single superparamagnetic microspheres in an external magnetic field. Phys Rev Lett 102:1–4
59. Liu Y, Chen H, Kenney LJ, Yan J (2010) A divalent switch drives H-NS/DNA-binding conformations between stiffening and bridging modes. Genes Dev 24:339–344
60. van der Valk RA, Vreede J, Qin L et al (2017) Mechanism of environmentally driven conformational changes that modulate H-NS DNA bridging activity. Elife 6:e27369
61. Kulić IM, Mohrbach H, Thaokar R, Schiessel H (2007) Equation of state of looped DNA. Phys Rev E Stat Nonlinear Soft Matter Phys 75:011913

62. Swinger KK, Rice PA (2004) IHF and HU: flexible architects of bent DNA. Curr Opin Struct Biol 14:28–35
63. Lin J, Chen H, Dröge P, Yan J (2012) Physical organization of DNA by multiple non-specific DNA-binding modes of integration host factor (IHF). PLoS One 7(11):e49885
64. Luger K, Mäder AW, Richmond RK et al (1997) Crystal structure of the nucleosome core particle at 2.8 A resolution. Nature 389: 251–260
65. Schalch T, Duda S, Sargent DF, Richmond TJ (2005) X-ray structure of a tetranucleosome and its implications for the chromatin fibre. Nature 436:138–141
66. Song F, Chen P, Sun D et al (2014) Cryo-EM study of the chromatin fiber reveals a double helix twisted by tetranucleosomal units. Science (80-) 344:376–380
67. Henneman B, Dame RT (2015) Archaeal histones: dynamic and versatile genome architects. AIMS Microbiol 1:72–81
68. Mattiroli F, Bhattacharyya S, Dyer PN et al (2017) Structure of histone-based chromatin in Archaea. Science (80-) 357:609–612
69. Hatch K, Danilowicz C, Coljee V, Prentiss M (2008) Measurement of the salt-dependent stabilization of partially open DNA by Escherichia coli SSB protein. Nucleic Acids Res 36: 294–299
70. Schäffet E, Nørrelykke SF, Howard J (2007) Surface forces and drag coefficients of microspheres near a plane surface measured with optical tweezers. Langmuir 23:3654–3665